BNL-113648-2017-JA

Suppressing Chromium Disproportion Reaction in O3-type Layered Cathode Material for High Capacity Sodium-ion Batteries

Ming-Hui Cao, Yong Wang, Zulipiya Shadike, Ji-Li Yue, Enyuan Hu, Seong-Min Bak, Yong-Ning Zhou, Xiao-Qing Yang, and Zheng-Wen Fu

Submitted to Journal of Materials Chemistry A

March 2017

Chemistry Department

Brookhaven National Laboratory

U.S. Department of Energy
USDOE Office of Science (SC)
USDOE Office of Energy Efficiency and Renewable Energy (EERE)

DISCLAIMER

Received 00th January 20xx,
Accepted 00th January 20xx

Suppressing Chromium Disproportion Reaction in O3-type Layered Cathode Material for High Capacity Sodium-ion Batteries

Ming-Hui Cao,[a] Yong Wang,[c] Zulipiya Shadike,[a] Ji-Li Yue,[a] Enyuan Hu,[d] Seong-Min Bak,[d] Yong-Ning Zhou*[b] and Xiao-Qing Yang*[d] and Zheng-Wen Fu*[a]

Chromium-based layered cathode materials suffer from the irriversible disproportion reaction of Cr^{4+} to Cr^{3+} and Cr^{6+}, which hinders the reversible multi-electron redox of Cr ions in layered cathodes, limits their capacity and reversibility. To address this problem, a novel O3-type layer-structured transition metal oxide of $NaCr_{1/3}Fe_{1/3}Mn_{1/3}O_2$ (NCFM) was designed and studied as a cathode material. A high reversible capacity of 186 mAh g^{-1} was achieved at a current rate of 0.05 C in a voltage range of 1.5 to 4.2 V. X-ray diffraction revealed a O3 → (O3+P3) → (P3+O3") → O3" phase-transition pathway for NCFM during charge. X-ray absorption, X-ray photoelectron and electron energy-loss spectroscopy measurements revealed the electronic structure changes of NCFM during Na^+ deintercalation/intercalation processes. It is confirmed that the disproportion reaction of Cr^{4+} to Cr^{3+} and Cr^{6+} can be effectively suppressed by Fe^{3+} and Mn^{4+} substitution. These results demonstrated that the reversible multi-electron oxidation/reduction of Cr ions can be achieved in NCFM during charge and discharge accompanied with CrO_6 octahedral distortion and recovery.

Introduction

The number of reports on studing the O3 layered $NaMO_2$ compounds (M = 3d transition metals such as Fe, Co, Ni, Mn, and Ti) with various M mixing has been of increased due to interesting electrochemical properties for sodium ion batteries (SIBs).[1] The synergistic effects of multiple transition metal cations in O3 layered structure have been demonstrated to improve the reversible capacity and to alter the charge/discharge curve.[2-12] Many efforts have been devoted to tuning the composition of different M mixing[2-12] and the substitution of Li[13] for M in order to achieve the high capacities and good cyclic performances for SIBs. Fe, Co, Ni, Cu Mn, and Ti were widely used in O3 compounds containing 2, 3, 4 or even 5 transition metal elements. These compounds included binary (e.g. $NaFe_{1/2}Mn_{1/2}O_2$,[2] $NaFe_{1/2}Co_{1/2}O_2$,[3] $NaNi_{1/2}Ti_{1/2}O_2$[4]), ternary (e.g. $NaNi_{1/3}Co_{1/3}Mn_{1/3}O_2$,[5] $NaNi_{1/3}Co_{1/3}Fe_{1/3}O_2$,[6] $NaNi_{1/3}Fe_{1/3}Mn_{1/3}O_2$,[7] $Na(Ni_{1/2}Mn_{1/2})_xFe_{1-x}O_2$[8] and $Na_{0.90}[Cu_{0.22}Fe_{0.30}Mn_{0.48}]O_2$[9]), quaternary (e.g. $NaNi_{0.25}Fe_{0.25}Co_{0.25}Mn_{0.25}O_2$[10] and $NaNi_{0.4}Fe_{0.2}Mn_{0.2}Ti_{0.2}O_2$[11]) and quinary ($NaNi_{1/4}Co_{1/4}Fe_{1/4}Mn_{1/8}Ti_{1/8}O_2$[12]) systems. However, to the best of our knowledge, no study has been reported on the sodium electrochemistry using layer-structured multi element $NaMO_2$ (M = transition metal) containing chromium for SIBs, although the O3-type layered $NaCrO_2$ was reported to be a potential cathode material for SIBs under a reversible Cr^{3+}/Cr^{4+} redox. It is known that the reversible capacity of O3-$NaCrO_2$ is about 120 mAh/g, corresponding to less than 0.5 sodium per $NaCrO_2$ extracted from the layered structure.[14,15] In previous studies, a partially reversible Cr^{3+}/Cr^{6+} redox in a manganese-chromium-based layered oxide $Li(Li_{0.2}Cr_{0.4}Mn_{0.4})O_2$ was reported for Li-ion batteries.[16,17] Therefore, it is worthwhile to explore the possibility of the three-electron redox couple of Cr^{3+}/Cr^{6+} in a layer-structured $NaMO_2$ cathode systems containing Cr element.

In this present work, we report the synthesis of a novel O3-type layered $NaCr_{1/3}Fe_{1/3}Mn_{1/3}O_2$ (denoted hereafter as NCFM) material, and the studies of its electrochemical properties in sodium cells. The phase transition behaviors and electronic structural changes of NCFM during charge and discharge are investigated by X-ray diffraction and absorption techniques. This O3-type NCFM can deliver a high reversible capacity approximately 186 mAh g^{-1} with relatively high coulombic efficiency for room temperature SIBs. These results demonstrate the feasibility of utilizing reversible Cr^{3+}/Cr^{6+} redox during charge/discharge process in O3-type layered $NaMO_2$ compounds and provided the valuable information about the structural changes of this material during charge-diacharge cycles.

Experimental Section

Material Synthesis

$NaFe_{1/3}Cr_{1/3}Mn_{1/3}O_2$ (NFCM) was synthesized by a conventional solid state reaction method. Stoichiometric amounts of Na_2O_2 (95% Alfa Aesar), Fe_2O_3 (99.99% Alfa Aesar), Mn_2O_3 (99.99% Alfa Aesar), and Cr_2O_3 (99.99% Alfa Aesar) powder were mixed by a mortar and pestle, then the mixture was pressed into a pellet. NFCM was synthesized by sintering the pellet at 900 °C in an argon gas flow for 12 h. The pellet was naturally cooled to room temperature and transferred immediately into an Ar-filled glovebox.

Material Characterization

[a] Shanghai Key Laboratory of Molecular Catalysis and Innovative Materials, Department of Chemistry & Laser Chemistry Institute, Fudan University, Shanghai, 200433, P.R. China. E-mail: zwfu@fudan.edu.cn
[b] Department of Materials Science, Fudan University, Shanghai, 200433, P.R. China. E-mail: zhouyongning@gmail.com
[c] Shanghai Institute of Space Power-Sources, Shanghai, 200245, P.R. China.
[d] Department of Chemistry, Brookhaven National Laboratory, Upton, New York 11973, USA. E-mail: xyang@bnl.gov
†Electronic Supplementary Information (ESI) available: [details of any supplementary information available should be included here]. See DOI: 10.1039/x0xx00000x

The morphology of the product was characterized by field emission scanning electron microscopy (SEM, Cambridge S-360). Powder X-ray diffraction (XRD) patterns were collected on an X-ray diffractometer (Bruker D8 Advance, Germany) with Cu-Kα radiation (λ = 0.1540 nm) at 40 kV, 40 mA. Data were obtained over the 2ϑ range of 10-70° for as-prepared materials and electrodes with a scan rate of 2° min^{-1}. X-ray absorption spectroscopy (XAS) was performed at beamline 12BM of Advanced Photon Source (APS) at Argonne National Laboratory. Cr, Fe, Mn K-edge XAS spectra were collected in transmission mode. The XAS data was processed using Athena and Artemis software packages.[18,19] The AUTOBK code was used to normalize the absorption coefficient, and to separate the EXAFS signal, $\chi(k)$, from the isolated atom-absorption background. The extracted EXAFS signal, $\chi(k)$, was weighted by k^3 to emphasize the high-energy oscillations and then Fourier-transformed in a k range from 3.5 to 11.5$Å^{-1}$ using a hanning window with a window sill (Δk) of 1.0 $Å^{-1}$, thereby obtaining magnitude plots of the EXAFS spectra in R-space (Å). The Fourier-transformed peaks were not phase-corrected, and thus the actual bond lengths are ~0.3-0.5 Å longer. The filtered Fourier transforms of EXAFS spectra were then fitted using theoretical single scattering paths generated with the FEFF 6.0 ab initio simulation code. XPS was performed on a Perkin Elmer PHI 5000C electron spectroscopy for chemical analysis (ESCA) system with monochromatic Al Kα (1486.6 eV) irradiation. The binding energies of samples were calibrated by taking the carbon C 1s peak as reference ~286.46 eV. A JEOL JEM-3010 transmission electron microscope operating at 300 keV with a LaB_6 filament equipped with a filed-emission gun and a parallel EELS spectrometer Gatan666 was used. Spectra were collected in TEM diffraction mode by the spectrometer using an illumination angle 2α = 4-10 mrad, a collection angle of 2b = 11.2 ± 0.3 mrad, a 2-mm diameter entrance aperture, and an energy dispersion of 0.1 eV/channel. The energy of the core-loss spectra was calibrated using the average position of the two zero-loss peaks. The position of the C-K (1s) peak at 284.9 ± 0.1 eV from the TEM a-C support film was used to evaluate the energy calibration.

Electrochemical Characterization

The working electrode was prepared by spreading the slurry of 70 wt % NFCM, 20 wt % carbon black, and 10 wt % polyvinylidenefluoride (PVDF, Sigma-Aldrich) on the aluminum foil. The electrodes were dried at 120°C for 12 h, and punched to small circular pieces with a diameter of 14 mm, the loading of the active material is about 1.8-2.1 mg cm^{-2}. Electrochemical cells were assembled in an Ar-filled glovebox (MBraun, Germany). The electrolytes consisted of 1 M $NaClO_4$ (Alfa-Aesar) in a nonaqueous solution of ethylene carbonate (EC, Alfa-Aesar) and propylene carbonate (PC, Alfa-Aesar) with a volume ratio of 1:1, 5 wt% fluroethylene carbonate (FEC) were added, according to the literature.[20,21] Galvanostatic charge-discharge measurements were carried out at room temperature on a Land CT 2001A battery test system by using coin cells. The coin cell were assembled with pure sodium foil as the counter electrode, and a glass fiber (Whatman GF/F) as the separator. The current density and specific capacity of electrodes were calculated on the basis of the weight of active materials.

Results and Discussion

Morphology and Structure Characterization

The crystal structure of the synthesized $NaCr_{1/3}Fe_{1/3}Mn_{1/3}O_2$ (NCFM) was analyzed by XRD and the pattern is shown in Figure 1(a). Rietveld refinement of the XRD pattern in Figure 1(a) confirmed that the structure of the as-prepared material is a hexagonal phase with a space group of R-3m. The lattice parameters are $a = b$ = 2.9639(4) Å, and c = 16.1693(5) Å. The low R-factors of R_p = 1.91%, R_{wp} = 2.9%, and GOF(χ^2) = 1.102 obtained for the Rietveld refinement indicates a good fit. The details of the structure parameter are shown in Table S1. These values are quite close to those reported in the literature for O3 type layered $NaMO_2$ oxides.[22,23] According to the XRD results, this O3-NCFM is the isostructure of α-$NaFeO_2$ and made of repeating labs of T_eO_6 (T_e = Cr, Fe, Mn) layers with Na ions being sandwiched between the oxide layers (Figure 1(b)). The oxygen atom layers are stacked in the order of ...ABCABC... arrangement, and all Na ions are in octahedral coordination with six oxygen ions. Scanning electron microscopy (SEM) images of the synthesized NCFM (Figure 1(c) and (d)) show the primary particles sizes are in the range of 0.5 - 1.0 µm.

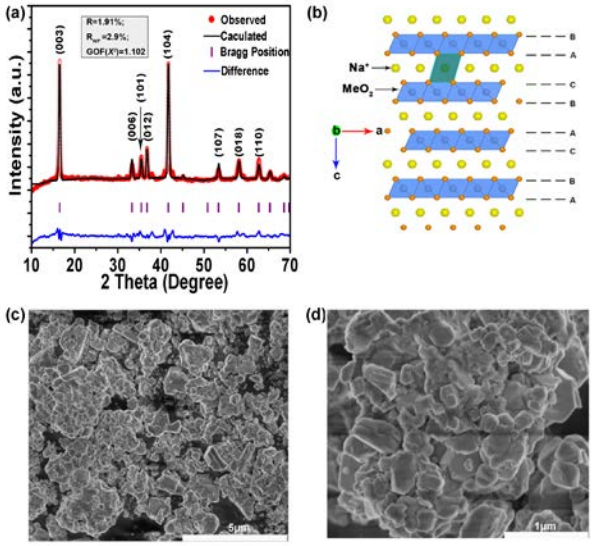

Figure 1. (a) Observed and calculated (Rietveld method) XRD pattern for the O3–NCFM. Red crosses: experimental, black line: calculated, blue line: difference and brown bars: Bragg positions; (b) schematic of the O3-NCFM crystal structure, legend: orange, blue and yellow balls stand for oxygen, transition metal and sodium ions, respectively; (c,d) SEM images of the as-prepared O3-NCFM.

Electrochemical properties

The galvanostatic cycling was performed to examine the sodium electrochemical behavior of NCFM, and its voltage-capacity profiles are presented in Figure 2(a). The open-circuit voltage (OCV) lies close to 2.7 V. In the initial charge process, a sloping voltage plateau from 2.95 to 3.75 V is observed and the initial charge capacity is found to be 194 mAh g^{-1} at a current density of 6 mA g^{-1}. During

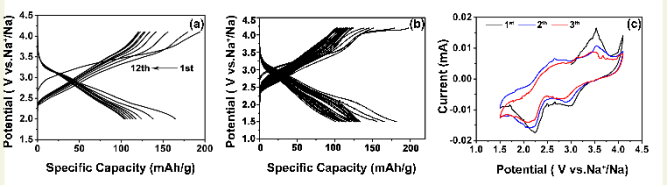

Figure 2. (a) Galvanostatic cycling curves of the NCFM electrode at a current rate of 0.03C (5mA g-1) in the potential range of 2.0–4.1 V versus Na+/Na; (b) Galvanostatic cycling curves of the NCFM electrode at a current rate of 0.05 C (10 mA g-1) in the potential range of 1.5–4.2 V versus Na+/Na; (c) First three cyclic voltammograms for the NCFM electrode cycled between 1.5 V and 4.1 V.

discharge, it can be seen that the initial discharge curve includes two sloping regions from 3.4 to 2.4 V and from 2.4 to 2.0 V. The inital discharge capacity is 165 mAh g^{-1}. The initial coulomb efficiency of 85% is observed. The charge/discharge capacities of the second, third, fifth and tenth cycles are 180/139 mAh g^{-1}, 156/123 mAh g^{-1}, 134/114 mAh g^{-1}, 122/105 mAh g^{-1}, respectively. Although large charge capacities of layered $NaMO_2$ can be achieved by increasing the cutoff voltage, their reversible capacities decrease obviously. For example, O3-type $NaCrO_2$ can only deliver a discharge capacity of 9 mAh g^{-1} when a high cutoff voltage of 4.5 V is used. In contrast, a reversible discharge capacity of 110 mAh g^{-1} can be achieved with a cutoff voltage of 3.5 V. [14] O3-type $NaFeO_2$ [24] and O'3-type $NaMnO_2$ [25] can provide reversible capacities of 80 mAh g^{-1} and 120~130 mAh g^{-1} respectively with suitable cutoff voltages less than 3.5 V. Apparently, the reversible capacity of NCFM electrode is much higher than that of $NaCrO_2$, $NaFeO_2$ or $NaMnO_2$. To evaluate the electrochemical behavior of NCFM in a wider voltage range, galvanostatic cycling was performed between 1.5 to 4.2 V, as shown in Figure 2(b). It can be seen that 0.81 Na, corresponding to a charge capacity of 198 mAh g^{-1}, can be de-intercalated from NCFM when the cell was charged to 4.2 V vs. Na/Na^+. Upon subsequent discharge to 1.5 V, 0.76 Na, corresponding to a discharge capacity of 186 mAh g^{-1} with high coulombic efficiencies of 94% can be reversibly re-intercalated back to the layered structure. Such a high capacity is very close to the highest capacity in all reported O3-type layered cathodes for SIBs (Table S2). In the subsequent cycles, the cell retained a reversible capacity of 127 mAh g^{-1} after 15 cycles and 100 mAh g^{-1} after 35 cycles in the voltage range of 1.5–4.2 V at a 0.05C rate, the coulombic efficiencies close to 90% are achieved in these subsequent cycles, indicating that the cyclability of NCFM is still poor and further improvements are needed. Figure 2(c) shows the first three cyclic voltammograms curves of NCFM electrode. There is a cathodic peak at 3.54 V in the initial charge process, indicating the first Na extraction process from NCFM. In the first discharge, two anodic peaks at 2.98 and 2.23 V are observed. Their corresponding cathodic peaks lie at 2.65 and 3.53 V in the second charge process. In the subsequent cycles, two couple of oxidation/reduction peaks at 3.45/2.88 V and 2.65/2.14 V corresponding to the reversible intercalation/deintercalation of Na ions in NCFM. Based on our results of previous studies, we would like to propose that the oxidation/reduction peaks at 2.65/2.14 V is corresponding to the Mn^{3+}/Mn^{4+} redox couple. This redox potential is close to of Mn^{3+}/Mn^{4+} in layered $Na_{2/3}(Fe_{1/2}Mn_{1/2})O_2$ (2.15/2.07V)[26] and in layered O3-$Na_xMn_{1/3}Fe_{2/3}O_2$ (2.4/2.3 V).[27] Previous studies showed that the potential of Cr^{3+}/Cr^{4+} redox couple in the layered $NaCrO_2$ is in the voltage range of 2.8-3.3 V vs. Na^+/Na,[28] while the reversible redox potential of Fe^{3+}/Fe^{4+} redox couple in $NaFeO_2$ [29] lies in the voltage range of 3.2-3.4 V. Therefore, the oxidation/reduction peaks at around 3.45/2.88 V could be attributed to the redox couple of Cr or Fe ions in NCFM.

X-ray diffraction (XRD) characterization

To investigate the phase transition behavior of NCFM during Na^+ intercalation and deintercalation, *ex situ* XRD patterns of NCFM were collected at various charge and discharge states during the first charge and discharge (shown in Figure 3). It can be seen that the (003) peak from XRD pattern of pristine NCFM is clearly observed as a single-fold peak. Every new (003) peak is a fingerprint for the formation of a new phase. The evolutions from other peaks of (006), (101), (012), and (104) during the charge and discharge process are difficult to detect due to their weak peak intensities. During the charge process, the (003) peak of the initial O3 phase shifts to lower angles with gradually decreased intensity when the amount of de-intercalacted Li changed from x = 0 to x = 0.2. At x = 0.1, a new (003) peak emerges, with increasing intensity and shifting position to lower angles when x values changing from x=0.1 to 0.5. As we know, the (003) peak is a single-fold peak. Thus, every new (003) peak is a fingerprint for the formation of a new phase. Combining with other peaks of (006), (101), (012), and (104), the new formed phase is more likely a P3 phase. It suggests that a phase transition from O3 to P3 phase at the earlier stage of charge takes place with the increasing interslab distance along c axis. This is a typical phase transition behavior for most of the O3-type layer-structured cathodes for SIBs during charge. Na ions extracted from the layered compounds lead to the increased repulsion force between the two neighbouring oxygen layers, causing the increased interslab distance during desodiation process. It is interesting to note that, another (003) peak representing a new O3 phase (labeled as O3") can be observed at x = 0.3, and shifts toward higher angles and becomes broader during further charge. Two-phase coexistence of P3 and O3" occurs at x > 0.3. When x values reaches 0.6, P3 phase starts to decrease and finally disappears at x = 0.8. A

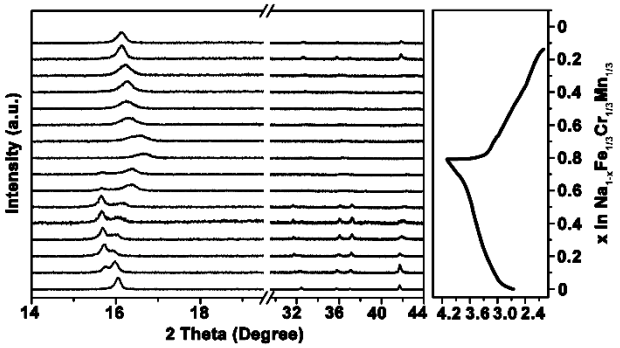

Figure 3. Ex situ X-ray diffraction patterns collected during the first charge and discharge processes of the Na/NCFM cells under a current rate of 10 mA g-1. The corresponding voltage-composition profile is shown on the right side of the XRD patterns.

very broad (003) peak of O3'' phase at x = 0.8 indicates severe structural distortion or a distribution of c lattice parameter of O3'' . The phase transition pathway of NCFM during the charge process is in the sequence of O3 → (O3+P3) → (P3+O3") → O3". Interestingly, the changes of of lattice parameter c for O3" phases is in the opposite direction for P3, when Na ions were removed from x = 0.3 to x = 0.7 during charge. This behavior is completely different than the previous reports behavior of O3-type layer-structured materials such as $NaCrO_2$,[30,31] $Na(Mn_{0.25}Fe_{0.25}Co_{0.25}Ni_{0.25})O_2$,[32] $NaFeO_2$–$NaNiO_2$,[33] $Na(NiCoFeTi)_{1/4}O_2$,[34] and $NaNi_{1/4}Co_{1/4}Fe_{1/4}Mn_{1/8}Ti_{1/8}O_2$[12]. In those systems, interslab distances were reported to be increased during most part of charging process, and changed to decrease only at the end of charging process. The phase transition of NCFM during discharge does not undergo an completely inversed way of the charge process, only involves the evolutions from O3" phase to O3 phase without the appearance of P3 phase.

X-ray absorption (XAS) characterization

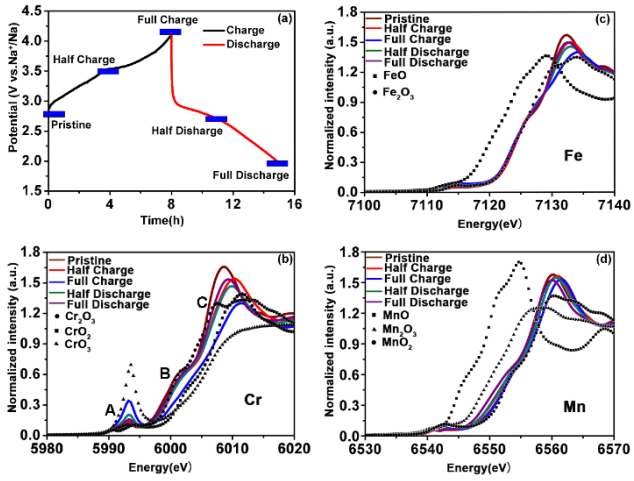

Figure 4. (a) Charge and discharge curve of the NCFM electrode during the first charge and discharge processes. Blue solid squares on the curve stand for the states where XAS data were collected. (b–d) Normalized XANES spectra of NCFM at various charge and discharge states during the first cycle at Cr, Fe, and Mn K-edges, respectively.

To further investigate the local structure and valence state changes of Cr, Fe, and Mn in the NCFM electrode during charge and discharge process, the *ex situ* X-ray absorption spectroscopy at the Cr, Fe, and Mn K-edge were carried out. The blue solid squares on the curve in Figure 4(a) marked the different states where XAS data were collected. Figure 4(b-d) show the K-edge X-ray absorption near edge spectroscopy (XANES) results for Fe, Cr, and Mn. Comparing the Cr, Fe and Mn k-edges XANES spectra of the pristine NCFM with the reference compounds $Cr_2O_3(Cr^{3+})$, $CrO_2(Cr^{4+})$, $FeO(Fe^{2+})$, $Fe_2O_3(Fe^{3+})$, $MnO(Mn^{2+})$, $Mn_2O_3(Mn^{3+})$, and $MnO_2(Mn^{4+})$, the absorption edges of Cr, Fe, and Mn at the pristine state are slightly lower than reference compounds Cr_2O_3, Fe_2O_3 and MnO_2, respectively. Thus, the oxidation states of Cr, Fe and Mn in the pristine NCFM could be estimated to be $Cr^{2+\text{ to }\sim3+}$, $Fe^{2+\text{ to }\sim3+}$, $Mn^{3+\text{ to }\sim4+}$, respectively.

When the electrode was charged, the shapes of Cr K-edge XANES at half and fully charged states are completely different from the pristine one (Figure 4(b)). They involve the increasing intensity of the pre-edge peak (denoted as A), the decreasing intensity of the edge peak (denoted as B), and a gradually shift of the edge peak (denoted as C) to higher energy from the pristine to fully charged states, indicating the oxidation of Cr^{3+} during Na ion extraction. A gradual intensity increase of the pre-edge peak A from the pristine to half and fully charged states are clearly observed, indicating the increase of the average oxidation state of the Cr ions after charging [17,35]. Based on the Cr pre-edge peak calibration reported by Peterson et al., [36] the average oxidation state of Cr ions after NCFM electrode charged to 4.1 V is estimated to be $Cr^{+4.2}$. To the best of our knowledge, this value is the highest average oxidation state of Cr reported up to now during charge in all chromium-based layered cathodes with reversible cycle performance. [14,15,37] For Fe and Mn K-edge spectra shown in Figure 4(c) and (d), it can be seen that both edges clearly shift toward higher energy during the charge process. By compared with the edge positions of reference compounds, the valence states of Fe and Mn after fully charge are estimated as Fe^{3+} and Mn^{4+}, respectively. Thus, the oxidation state change of Fe ions indicates that the Fe and Mn ions are both active when the cells are cycled in the voltage range of 1.5-4.1 V. Upon discharge, the XANES spectra of Cr, Fe and Mn undergo evolutions in the opposite direction to the charge process. The edge positions can completely return to their pristine states after discharge, indicating the reversible valence state changes of Cr, Fe and Mn in NCFM, However, the shape of spectra cannot be fully recovered, suggesting the surrounding environments of the transition metal ions are not fully restored. Apparently, the charge compensation in the NCFM material is achieved by the $Cr^{3+}/Cr^{4.2+}$, $Fe^{2+\text{ to }\sim3+}/Fe^{3+}$, $Mn^{2+\text{ to }\sim3+}/Mn^{4+}$ redox couples during the desodiation and sodiation processes.

The detailed structural parameters of NCFM at different charge/discharge states can be obtained by fitting the first two peaks of the Fourier transformed Cr, Fe and Mn K-edge EXAFS spectra and are listed in Table S3-S5. For the pristine NCFM, the Cr-O distance from the Cr-O shell with Cr surrounded by six oxygen atoms is 1.99 Å. This value is very close to the Cr-O distance of 2.00 Å reported in layered O3-$NaCrO_2$, [38] in which Cr ions occupy octahedral sites in the hexagonal lattice. Interatomic distances of Fe-O and Mn-O are 2.03 and 1.90 Å, respectively. These values are close to the estimated values of the 2.05 Å for Fe-O [39] and 1.94 Å for Mn-O [40] in the octahedral environment, respectively. These results confirm the octahedral site occupation of Fe, Cr, Mn in the pristine NCFM. It can be seen that Cr-O, Fe-O and Mn-O bond lengths all decrease during charging, which are due to the oxidation of transition metal ions during Na^+ deintercalation. It should be noted that at the end of charge the bond lengths of Cr-O and Mn-O decrease only slightly from 1.99 to 1.97 Å and 1.90 to 1.89 Å, respectively, while the bond length of Fe-O decreases drastically from 2.03 to 1.96 Å, indicating the Fe ions are electroactive. [41] However, all of the bond lengths cannot fully return to their original states after discharge, possibly due to the residues of octahedral distortion.

Electron energy-loss spectroscopy (EELS) and X-ray photoelectron spectroscopy (XPS) characterization

EELS and XPS techniques were used to identify the oxidation state of Cr in the NCFM electrode. Figure 5 present Cr $L_{2,3}$ edges of EELS and Cr 2p XPS spectra of the NCFM electrode after charging to 4.1 V. For comparison, EELS and XPS spectra of the standards from $K_2Cr_2O_7$, $KCr(SO_4)_2{\cdot}12H_2O$ and CrO_2 are also included. It can be found that both EELS and XPS data from reference compounds are congruous with previous literatures,[42,43] respectively. As shown in

Figure 5(a), one pair of Cr–L2 and Cr–L3 edges in the EELS spectrum is observed and Cr L3 core level peak position is located at 580.04 eV. This value is less than that of the L3 peak from $K_2Cr_2O_7$ (Cr^{6+}) at

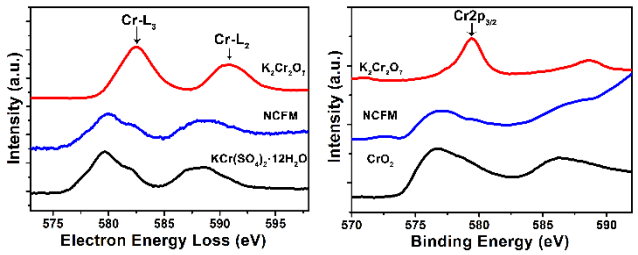

Figure 5 (a) Cr $L_{2,3}$ edges of electron energy loss spectra from the NCFM electrode after charging to 4.1 V, and from the standards of $K_2Cr_2O_7$ and $KCr(SO_4)_2.12H_2O$; (b) Cr 2p XPS spectra of the NCFM electrode after the charging to 4.1 V, and from the standards of $K_2Cr_2O_7$ and CrO_2.

582.50 eV, and is higher than that of the L3 peak from $KCr(SO_4)_2{\cdot}12H_2O$ (Cr^{3+}) at 579.70 eV, supporting that the oxidation state of the Cr ions from the NCFM electrode after the charging to 4.1 V is in the rangs from 3^+ to 6^+. This is further confirmed by XPS data shown in Figure 5(b), in which the Cr $2p_{3/2}$ peaks from XPS spectra of NCFM, CrO_2 (Cr^{4+}), and $K_2Cr_2O_7$ (Cr^{6+}) are found to be 577.0 eV, 576.8 eV, and 579.4 eV, respectively. If compared with Cr $2p_{3/2}$ peak from XPS spectrum of CrO_2, there is a small peak shift of 0.2 eV toward high energy from that of desodiated NCFM electrode, implying that the oxidation state of the Cr ions in the desodiated NCFM electrode is little higher than +4. These results are in accord with XAS data in Figure 4.

Based on the previous studies, [17] Cr ions in $Cr^{3+}(d^3)$ and $Cr^{6+}(d^0)$ configurations are more stable than those in Cr^{4+} (d^2) configuration, so Cr ions in layered compounds mostly exist as Cr^{3+} or Cr^{6+}. A disproportion reaction of Cr^{4+} in layered structure was proposed as below:

$$3\,Cr^{4+} \rightarrow 2Cr^{3+} + Cr^{6+} \qquad (1)$$

Generally, Cr^{3+} and Cr^{4+} ions often occupy the sites octahedrally coordinated with oxygen, while Cr^{6+} with smaller ionic size occupies in sites tetrahedrally coordinated with oxygen as shown in Figure 6.[17,44] As proposed by Bo and Ceder et al.[45], the Cr^{4+} disproportionation is coupled with charge transfer of three Cr^{4+} in close proximity likely Cr^{4+} triplets and the mobility of one Cr^{4+} among triplets from octahedral sites to its nearest-neighbor interstitial tetrahedral sites (Cr^{6+}). For the desodiated O3-NCFM, the

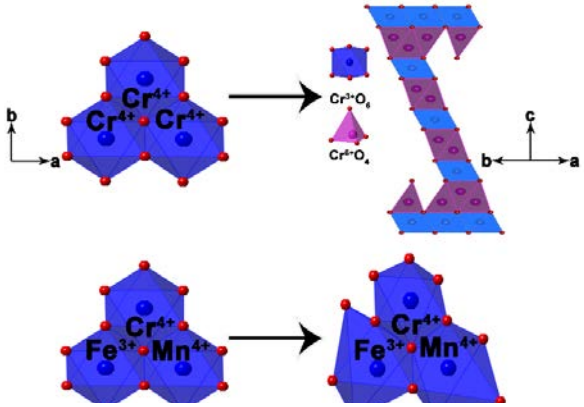

Figure 6. Schematic of a suppressing disproportionation mechanism of Cr^{4+} in NCFM material during desodiation/sodiation.

transition metals of Cr, Fe and Mn are assumed to be homogeneously distributed in the octahedral sites. Two thirds Cr^{4+} in Cr^{4+} triplets will be replaced by Mn^{4+} and Fe^{3+} (Figure 6). Because the electronegativity of Fe^{3+} is less than that of Cr^{4+} (Table S6), the electron transfer from Cr^{4+} to Fe^{3+} is blocked, implying that the disproportionation reaction is suppressed. This is evidenced by XAS, EELS and XPS data, in which the valence state of Cr from the desodiated O3-NCFM should be close to +4 instead of +6. The octahedron of $Cr^{4+}O_6$ is locally distorted because Cr^{4+} ions have the $t_{2g}^2\ e_g^0$ configuration (see Figure S1), which are Jahn-Teller active due to the uneven occupation of the t_{2g} orbitals. This is in good agreement with the very broad (003) peak of O3'' phase at $x = 0.8$ in XRD patterns. Two (axial) Cr–O bonds are elongated whereas four (planar) Cr–O bonds are shortened. The Jahn–Teller effect of Cr^{4+} are convinced by the low intensities of the Cr-O and Cr-TM peaks of the FT-EXAFS spectra associated with decreased coordination number of Cr atoms after the full charging (as shown in Figure S2). The formation of Jahn-Teller distorted CrO_6 octahedral at the high voltage region can significantly lowers the Na diffusion barrier, improving Na mobility at the top of charge [42]. In contrast, the intensities of the Fe-O (Figure S3) and Mn-O (Figure S4) peaks of the FT-EXAFS spectra are not changed. These results suggest that the coordination numbers of nearest neighbors coordinated Fe or Mn atoms remain about 6, so the local distortion of FeO_6 and MnO_6 is indeed much weaker than that of CrO_6. Such a structure configuration can effectively suppress Cr^{4+} disproportionation reaction, and facilitate the multi-electron oxidation/reduction process of $Cr^{3+}/Cr^{4.2+}$ in the O3-type layered NCFM with a large reversible capacity.

Conclusions

In summary, a novel O3-type layered NCFM was synthesized as a cathode material for Na-ion batteries. The electrochemical characterization shows a reversible specific capacity of 165 mAh g−1 in a voltage range of 2–4.1 V and 186 mAh g−1 in a voltage range of 1.5–4.2 V. X-ray diffraction and Cr, Fe and Mn K-edge XAS measurements clarified that $Cr^{3+}/Cr^{4.2+}$, $Fe^{2+\ to\ \sim3+}/Fe^{3+}$, $Mn^{2+\ to\ \sim3+}/Mn^{4+}$ redox couples are involved during the desodiation and sodiation processes. An interesting multi-electron reaction of $Cr^{3+}/Cr^{4.2+}$ in NCFM material is revealed while $Cr^{4.2+}$ can be stabilized at octahedral sites with the small distortion of $Cr^{4.2+}O6$. The gradual distortion of CrO6 octahedral might be related to the evolution of O3'' phase during the desodiation and sodiation processes. The disproportion reaction of Cr^{4+} is effectively suppressed by Fe^{3+} and Mn^{4+} substitution. The NCFM can be used as the cathode material for rechargeable sodium ion batteries and provide a novel case to understand the multi-electron electrochemistry in O3-type layered materials. The high reversible capacities of Cr-based O3-type layered cathodes may open a promising approach to search for high energy density cathode materials for sodium ion batteries.

Acknowledgements

This work was financially supported by the NSAF (Grant No. 51502039 and U1430104), the National Key Scientific Research Project (Grant No. 2016YFB090150), 1000 Youth Talents Plan and Science & Technology Commission of Shanghai Municipality (08DZ2270500). The work at

Brookhaven National Laboratory was supported by the Assistant Secretary for Energy Efficiency and Renewable Energy, Office of Vehicle Technologies of the U.S. Department of Energy through the Advanced Battery Materials Research (BMR) Program under Contract No. DE-SC0012704. The authors thank technical supports by beamline scientists Sungsik Lee and Benjamin Reinhart at 12BM of Advanced Photon Source at Argonne National Laboratory, supported by the U.S. Department of Energy, Basic Energy Science, under Contract No. DE-AC02-06CH11357. The authors also thank beamline BL14W1 of the Shanghai Synchrotron Radiation Facility (SSRF).

Notes and references

[1] M. H. Han, E. Gonzalo, G. Singh and T. Rojo, *Energy Environ. Sci*. 2015, **8***,* 81.
[2] N. Yabuuchi, M. Kajiyama, J. Iwatat, H. Nishikawa, S. Hitomi, R. Okuyama, R. Usui, Y. Yamada and S. Komaba, *Nat. Mater.* 2012, **11**, 512.
[3] H. Yoshida, N. Yabuuchi and S. Komaba, *Electrochem. Commun.* 2013, **34,** 60.
[4] H. J. Yu, S. H. Guo, Y. B. Zhu, M. Ishida and H. S. Zhou, *Chem. Commun.* 2014, **50**, 457.
[5] M. Sathiya, K. Hemalatha, K. Ramesha, J.-M. Tarascon and A. S. Prakash, *Chem. Mater.* 2012, **24**, 1846.
[6] P. Vassilaras, A. J. Toumar and G. Ceder, *Electrochem. Commun.* 2014, **38**, 79.
[7] D. Kim, E. Lee, M. Slater, W. Lu, S. Rood and C.S. Johnson, *Electrochem. Commun.* 2012, **18**, 66.
[8] D. D. Yuan, Y. X. Wang, Y. L. Cao, X. P. Ai and H. X. Yang, *ACS Appl. Mater. Interfaces* 2015, **7**, 8585.
[9] L. Q. Mu, S. Y. Xu, Y. M. Li, Y. S. Hu, H. Li, L. Q. Chen and X. G. Huang, *Adv. mater.* 2015, **27,** 6928.
[10] X. Li, D. Wu, Y. N. Zhou, L. Liu, X. Q. Yang and G. Ceder, *Electrochem. Commun.* 2014, **49,** 51.
[11] X. Sun, Y. Jin, C. Y. Zhang, J. W. Wen, Y. Shao, Y. Zang and C. H. Chen, *J. Mater. Chem. A* 2014, **2**, 17268.
[12] J. L. Yue, W. W. Yin, M. H. Cao, S. Zulipiya, Y. N. Zhou and Z.W. Fu, *Chem.Comm.* 2015, **51**, 15712.
[13] J. Xu, H. Liu, Y. S. Meng, *Electrochem. Comm*. 2015, **60**, 13.
[14] K. Kubota, I. Ikeuchi, T. Nakayama, C. Takei, N. Yabuuchi, H. Shiiba, M. Nakayama and S. Komaba, *J. Phys. Chem. C.* 2015, **119**, 166.
[15] C. Y. Yu, J. S. Park, H.G. Jung, K.Y. Chung, D. Aurbach, Y.K. Sun and S. T. Myung, *Energy Environ. Sci.* 2015, **8**, 2019.
[16] Z. Lu, and J. R. Dahn, *J. Electrochem. Soc.* 2003, **150**, A1044.
[17] M. Balasubramanian, J. McBreen, I. J. Davidson, P. S. Whitfield, and I. Kargina, *J. Electrochem. Soc.* 2002, **149**, A176.
[18] Newville, M. *J. Synchrotron Radiat.* 2001, **8**, 322.
[19] B. Ravel and M. Newville, *J. Synchrotron Radiat*. **2005**, *12*, 537.
[20] S. Komaba, T. Ishikawa, N. Yabuuchi, W. Murata, A. Ito and Y. Ohsawa, *ACS Appl. Mater. Interfaces* 2011, **3**, 4165.
[21] B. Mortemard de Boisse, J. H. Cheng, D. Carlier, M. Guignard, C. J. Pan, S. Bordere, D. Filimonov, C. Drathen, E. Suard, B. J. Hwang, A. Wattiauxa and C. Delmas, *J. Mater. Chem. A* 2015, **3**, 10976.
[22] A. C. Larson and R. B. Von Dreele, *General Structure Analysis System*, LANSCE, MS-H805, Los Alamos, New Mexico 1994.
[23] B. H. Toby, *J. Appl. Crystallogr.* 2001, **34**, 210.
[24] J. Zhao, L. Zhao, N. Dimov, S. Okada and T. J. Nishida, *Electrochem. Soc.* 2013, **160**, A3077.
[25] X. Ma, H. Chen and G. J. Ceder, *Electrochem. Soc.* 2011, **158**, A1307.
[26] W. K. Pang, S. Kalluri, V. K. Peterson, N. Sharma, J. Kimpton, B. Johannessen, H. K. Liu, S. X. Dou and Z. P. Guo, *Chem. Mater*. 2015, **27**, 3150.
[27] B. Mortemard de Boisse, D. Carlier, M. Guignard, and C. Delmas, *J. Electrochem. Soc.* 2013, **160**, A569.
[28] J. J. Ding, Y. N. Zhou, Q. Sun and Z. W. Fu, *Electrochem.Commun*. 2012, **22**, 85.
[29] N. Yabuuchi, H. Yoshida, and S. Komaba, *Electrochemistry* 2012, **80**, 716.
[30] Y.N. Zhou, J.J. Ding, K. W. Nam, X. Yu, S. M. Bak, E. Hu, J. Liu, J. Bai, H. Li, Z. W. Fu and X. Q. Yang, *J. Mater. Chem. A,* 2013, **1**, 11130.
[31] S. Komaba, T. Nakayama, A. Ogata, T. Shimizu, C. Takei, S. Takada, A. HokuraanI and Nakai, *Ecs Transactions* 2008, **16**, 43.
[32] X. Li , D. Wu , Y.N. Zhou , L. Liu, X.Q. Yang and G. Ceder, *Electrochem. Commun.* 2014, **49**, 51.
[33] X. Wang. G. Liu, T. Iwao. M. Okubo. and A. Yamada, *J. Phys. Chem. C* 2014, **118**, 2970.
[34] J. L. Yue, Y. N Zhou, X. Yu, S.M. Bak, X.Q. Yang and Z. W. Fu, *J. Mater. Chem. A* 2015, **3**, 23261.
[35] B. A. Manning, J.R. Kiser, H. Kwon and S. R. Kanel, *Environ. Sci. Technol.* 2007, **41**, 586.
[36] M.L. Peterson, G. E. Brown, J R., G. A. Parks and C. L L. *Stein Geochimica et Cosmochimica Acta*, 1997, **61**, 3399.
[37] Y. Wang, R. Xiao, Y.S. Hu, M. Avdeev and L. Chen, Nat. Commun., DOI: 10.1038/ncomms7954
[38] K. Kubota, I. Ikeuchi, T. Nakayama, C. Takei, N. Yabuuchi, H. Shiiba, M. Nakayama and S. Komaba, *J. Phys. Chem. C* 2015, **119**, 166.
[39] N. Yabuuchi, H.i Yoshida and S. Komaba, *Electrochemistry* 2012, **80**, 716.
[40] O. I. Velikokhatnyi, C.-C. Chang and P. N. Kumtaa, *J. Electrochem. Soc.* 2003,**150**, A1262.
[41] Y. W. Tsai, B. J. Hwang, G. Ceder, H. S. Sheu, D. G. Liu and J. F. Lee, *Chem. Mater.* 2005, **17***,* 3191.
[42] T.L. Daulton and B.J. Little,*Ultramicroscopy* 2006**, 106***,* 561.
[43] T. L. Daulton,B. J. Little, K. Lowe and J. J. Meehan, *Journal of Microbiological Methods* 2002**, 50**, 39.
[44] N.K. Karana, M. Balasubramanianb, D. P. Abrahamc, M. M. Furczonc, D.K. Pradhand, J. J. Saavedra-Arias, R. Thomas and R. S. Katiyar, *J. Power Sources* 2009, **187**, 586.
[45] X. Li, Y. Wang, D. Wu, L. Liu, S. -H. Bo and G. Ceder, *Chem. Mater.* 2016, **28**, 6575.

GRAPHICAL ABSTRACT

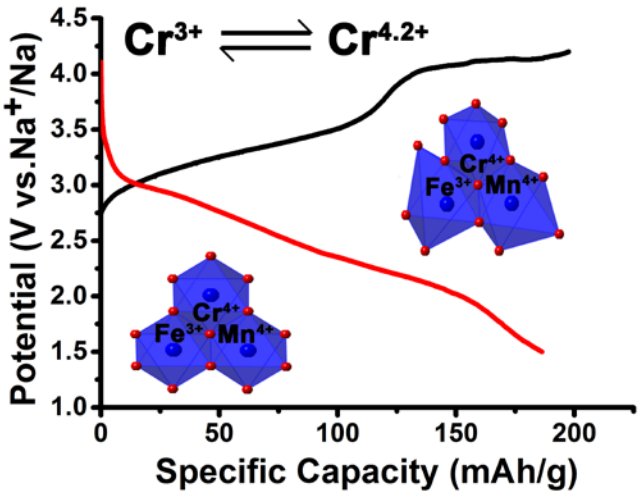

The reversible multi-electron oxidation/reduction process of $Cr^{3+}/Cr^{4.2+}$ with a large reversible capacity can be achieved in a novel O3-type layer-structured transition metal oxide of $NaCr_{1/3}Fe_{1/3}Mn_{1/3}O_2$. The disproportion reaction of Cr^{4+} to Cr^{3+} and Cr^{6+} can be effectively suppressed by Fe^{3+} and Mn^{4+} substitution during charge and discharge accompanied with CrO_6 octahedral distortion and recovery.